The Astronomical Journal, 125:3222–3236, 2003 June

DISCOVERY OF A LITTLE HOMUNCULUS WITHIN THE HOMUNCULUS NEBULA OF η CARINAE[1]

Kazunori Ishibashi,[2,3] Theodore R. Gull,[2,4] Kris Davidson,[5] Nathan Smith,[5,6] Thierry Lanz,[2,7] Don Lindler,[2,8] Keith Feggans,[2,8] Ekaterina Verner,[2,9] Bruce E. Woodgate,[2,4] Randy A. Kimble,[2,4] Charles W. Bowers,[2,4] Steven Kraemer,[2,4,9] Sarah R. Heap,[2,4] Anthony C. Danks,[2,4,10] Stephen P. Maran,[4,11] Charles L. Joseph,[4,12] Mary Elizabeth Kaiser,[4,13] Jeffrey L. Linsky,[4,14] Fred Roesler,[4,15] and Donna Weistrop[4,16]

Received 2002 December 26; accepted 2003 March 12

ABSTRACT

We report long-slit spectroscopic mapping of the η Carinae nebula obtained using the Space Telescope Imaging Spectrograph. The observations reveal the presence of a previously unknown bipolar emission nebula (roughly $\pm 2''$ along its major axis) embedded within the well-known and larger Homunculus Nebula. A preliminary analysis suggests that this embedded nebula may have originated from a minor eruption event circa 1890, 50 years after the formation of the larger Homunculus.

Key words: circumstellar matter — ISM: individual (Little Homunculus) — ISM: jets and outflows — stars: individual (η Carinae) — stars: mass loss — stars: winds, outflows

1. INTRODUCTION

Observed proper motions confirm that the major eruption of η Carinae seen in the 1840s produced the two main lobes of the Homunculus Nebula (Gaviola 1950; Ringuelet 1958; Morse et al. 1998; Smith & Gehrz 1998; Currie & Dowling 1999). Some features outside the Homunculus, however, were very likely ejected earlier (Walborn, Blanco, & Thackeray 1978). Apparently, η Car may have undergone a number of episodic outbursts before the major eruption (see Davidson & Humphreys 1997 and references therein). At least two questions arise: Do all of the star's outbursts eventually produce recognizable nebular features? Do all such features tend to have a similar bipolar (quasi-axial) geometry?

The historical light curve indicates a secondary eruption during the 1890s (Humphreys, Davidson, & Smith 1999). Some detectable equatorial material probably originated in that later event (Smith & Gehrz 1998; Davidson et al. 2001), but cannot easily be identified in continuum *Hubble Space Telescope* (*HST*) WFPC2 images (Morse et al. 2001). Here we report the detection and preliminary analysis of a relatively small bipolar structure *inside* the central regions of the familiar Homunculus lobes, and most likely ejected in the 1890 event. This mini-homunculus became evident in spectroscopic data obtained with the Space Telescope Imaging Spectrograph (STIS).

2. DISCOVERY OF THE NEW BIPOLAR NEBULA

We first noticed a previously unknown velocity structure near η Car in *HST* STIS spectroscopy obtained on 1998 March 19. Initially the geometric details were not clear, and we referred to it as the "integral-sign nebula ($\oint$)" (Gull et al. 1999; Ishibashi 1999). Figure 1 illustrates the $52'' \times 0\farcs1$ aperture orientation for those observations, position angle 152.°1–332.°1. In programs to monitor the star's 5.5 yr spectroscopic cycle and to explore the Homunculus, we obtained similar data on later occasions, listed in Table 1. Because of *HST* scheduling constraints, the slit orientation differed from the bipolar axis direction by about 20°. Figure 2 shows the appearance of emission lines within $2''$ of the star in the 1998 data; the right-hand part is a median-filter superposition of more than 30 lines, mostly [Fe II], in the 4000–5000 Å spectral interval.

The velocity structure has two obvious components extending from $-2''$ to $+2''$ across the star: a narrow straight part at $V \approx -32$ km s^{-1} (heliocentric), and a narrow, curved component with peak velocities $V \sim \pm 200$ km s^{-1}. Hereafter we call these the bar and curve components, respectively. The latter appears to be approximately symmetric around the stellar position, suggestive of a bipolar geometry. The bar

[1] Based on observations made with the NASA/ESA *Hubble Space Telescope*, and supported by GO grants 7302 and 8327 from the Space Telescope Science Institute and STIS GTO funding. This paper is a merger of the *HST* GO programs (PI: K. Davidson) and STIS IDT Key Project 8483, which used orbits allocated in the shared Guaranteed Telescope Observations. The STScI is operated by the Association of Universities for Research in Astronomy, Inc., under NASA contract NAS 5-26555.

[2] Laboratory for Astronomy and Solar Physics, Code 681, NASA Goddard Space Flight Center, Greenbelt, MD 20771.

[3] Current address: Center for Space Research, Massachusetts Institute of Technology, NE80-6011, 77 Massachusetts Avenue, Cambridge, MA 02139; bish@space.mit.edu.

[4] Co-investigator of the Space Telescope Imaging Spectrograph Instrument Definition Team.

[5] Department of Astronomy, University of Minnesota, Minneapolis, MN 55455.

[6] Current address: Center for Astrophysics and Space Astronomy, 389 UCB, University of Colorado, Boulder, CO 80309.

[7] Department of Astronomy, University of Maryland, College Park, MD 20742.

[8] Advanced Computer Concepts, Inc., 11518 Gainsborough Road, Potomac, MD 20854-6096.

[9] Department of Physics, Catholic University of America, Washington, DC 20064.

[10] SGT, Inc., Suite 400, 7701 Greenbelt Road, Greenbelt, MD 20770.

[11] Space Sciences Directorate, Code 600, NASA Goddard Space Flight Center, Greenbelt, MD 20771.

[12] Rutgers University, Physics and Astronomy Department, 136 Frelinghuysen Road, Piscataway, NJ 0855-0849.

[13] Department of Physics and Astronomy, Johns Hopkins University, 3400 North and Charles Street, Baltimore, MD 21218.

[14] Joint Institute for Laboratory Astrophysics, Campus Box 440, University of Colorado, Boulder, CO 80309-0440.

[15] Department of Physics, University of Wisconsin, 1150 University Avenue, Madison, WI 53711.

[16] Department of Physics, University of Nevada, Las Vegas, 4505 Maryland Parkway, Las Vegas, NV 89154-0804.

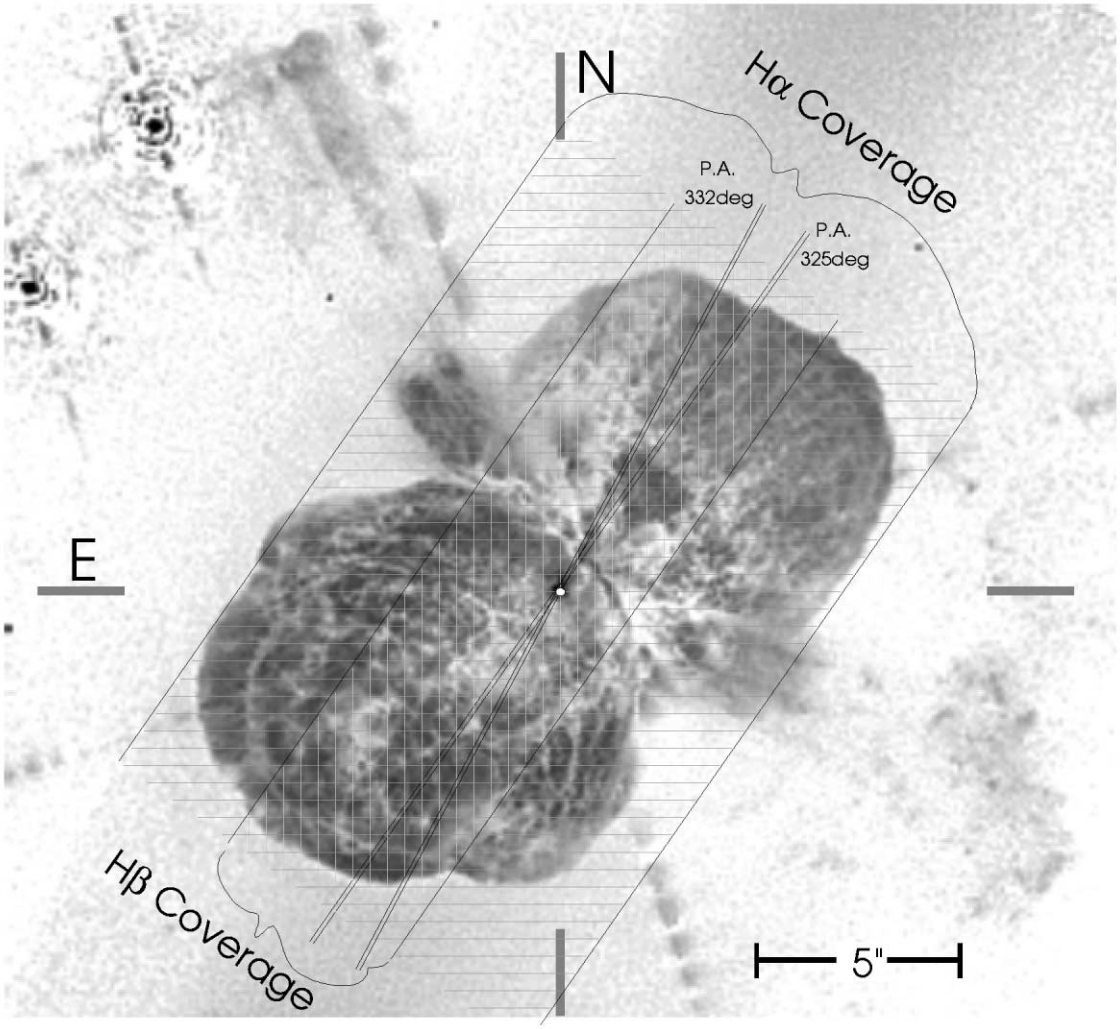

FIG. 1.—Orientation, size, and mapping coverage of the STIS slit used for these observations. The *HST* WFPC2 image shown here was obtained in 1995, but its scale has been adjusted slightly to allow for expansion to 1998.3 epoch. Its brightness has also been adjusted to bring out the nebular ejecta.

component, on the other hand, may represent expanding gas located outside the Homunculus lobes (see § 4.3).

Figure 3 shows [Ni II] λ7380 (in vacuum) velocity structures along the slit, observed 2000 March 13 with a slit orientation closer to the major axis. Some of these were sketched earlier in Figure 2*d* of Davidson et al. (2001).[17] Components 1 and 2 represent intrinsic emission in the southeast and northwest Homunculus lobes, while 3 is light reflected by dust grains in the polar region of the southeast lobe. Segments 4 and 5 are equatorial emission structures with ages of roughly 160 and 100 yr, respectively (see also Zethson et al. 1999). In this paper, however, we are concerned with the additional components 6 and 7, the curve component of the central structure, shown with a very different aspect ratio in Figure 2. The bar component is not conspicuous in Figure 3.

[17] For the same reason as in the earlier paper, to avoid ambiguity, here we use the term "apparent Doppler velocity" instead of "radial velocity." Quoted values are heliocentric.

TABLE 1
RELEVANT *HST* STIS OBSERVATIONS OF η CARINAE

Visit	Date	MJD	Slit P.A. (deg)	Aperture (arcsec)	Target
2.....	1998 Mar 19	50891.7	332.06	52 × 0.1	star
4.....	1999 Feb 21	51230.5	332.11	52 × 0.1	star
5.....	2000 Mar 13	51616.5	318.86	52 × 0.2 F1[a]	bipolar axis
6.....	2000 Mar 20	51623.8	332.11	52 × 0.1	star
7.....	2000 Mar 21	51624.3	325.06	52 × 0.1	mapping

[a] The central star is occulted with a coronagraphic bar F1 in this observation.

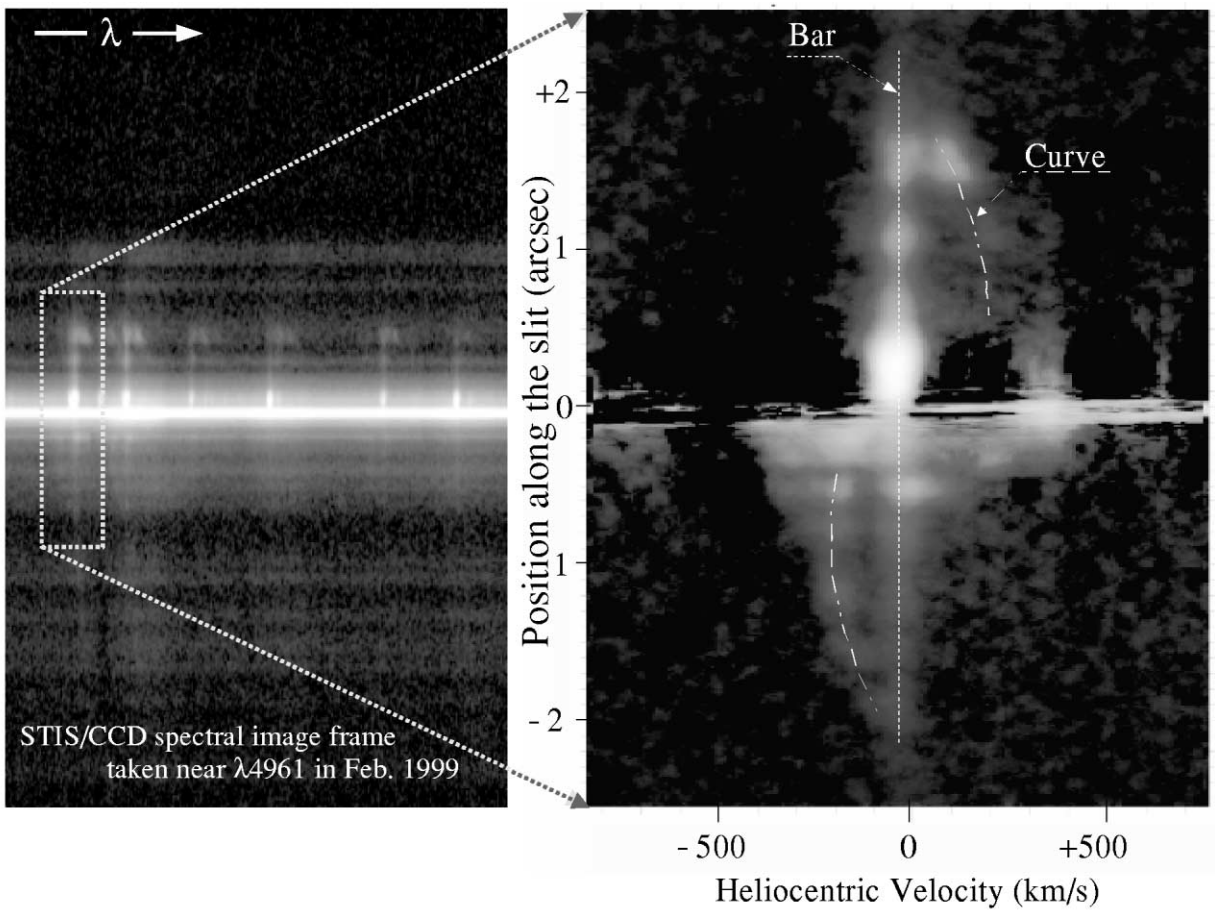

FIG. 2.—Two-dimensional spectral images of the newly discovered nebula embedded within the Homunculus Nebula. *Left*: A spectral image of the narrow, bright emission lines. *Right*: Median composite of 30 unblended [Fe II] and [Ni II] lines. The original spectra were recorded 1998 March 29 at slit position angle 332°.06.

Gull et al. (1999) and Ishibashi (1999) initially speculated that the small internal nebula was a narrow, collimated bipolar flow. This hypothesis was based on the early 1998 data, with one particular slit position angle. In order to check or improve the original model, it was imperative to obtain a spectral map of the region with additional slit positions. The STIS Instrument Development Team allocated four *HST* orbits to this mapping activity as a key GTO project. The mapping visit was executed in late March 2000 (visit 7 in Table 1). Results are described in the following section.

3. MAPPING OBSERVATIONS

Spectroscopic mapping near η Car was achieved on 2000 March 21 with the *HST* STIS CCD, using STIS gratings G430M and G750M at standard tilts that sampled wavelength ranges 4820–5100 Å (blue) and 6490–7050 Å (red) (Kimble et al. 1998; Woodgate et al. 1998). The $52'' \times 0''.1$ slit, oriented at position angle 145°.1 ↔ 325°.1, was placed at various locations, and exposure times were typically 80 s each. Figure 1 shows one of the slit positions and also the total spatial coverage at each central wavelength. The blue mapping extended from 2″.9 NE to 1″.9 SW (measured perpendicular to the slit) at 0″.1 intervals. The red mapping spanned a width of 12″ at 0″.05–0″.25 intervals. Several positions close to η Car were resampled at shorter exposures because of severe saturation of Hα and Hβ. Spectral resolutions were approximately 32 and 47 km s^{-1} for the red and blue mappings, respectively.

Our scientific goals required high-precision astrometry and spectroscopy with the data set. As we were pushing the diffraction limit of the telescope in our extractions, routine pipeline calibration was inadequate. We performed our own recalibration with special tools developed by one of us (K. I.) and by the STIS IDT group. The key steps were (1) spatial alignment of all spectral images with an accuracy of about 0″.013, a quarter of the raw CCD pixel size, including corrections for thermal effects in the STIS instrument (see Gull et al. 1997); (2) improved spectral image rectification in order to correct for a tilt in each spectral image; and (3) correction for wavelength offsets to an accuracy of $\sim\pm 7$ km s^{-1}. These correction steps were applied to derive input parameters used in the STIS IDT data reduction program CALSTIS (version 6.6; see Lindler 1999[18]).

We did not use hydrogen and helium lines in the analysis of the velocity structure, since their narrow intrinsic components are blended with broader scattered components. We therefore focused our attention on the [Fe II] lines, which are ubiquitous and narrow in the spectrum of the Homunculus.

[18] See http://hires.gsfc.nasa.gov/stis/docs/calstis/calstis.html.

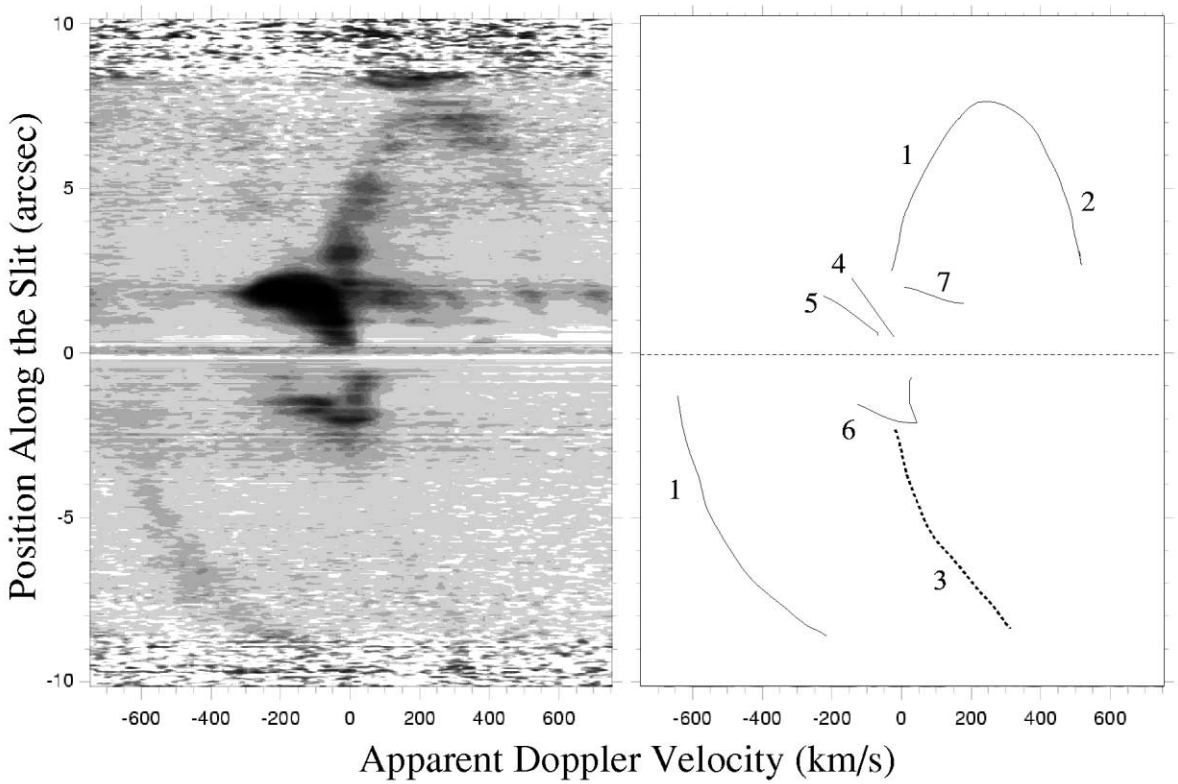

FIG. 3.—*Left*: Deep spectral image of the Homunculus and its internal bipolar nebula at [Ni II] λ7380 (vacuum). The brightest features are shown in dark color. *Right*: Tracing of nebular features seen in the spectral map. Intrinsic emission is marked by a solid line (scattered emission by a dashed line). These features are: (1) and (2) the side and caps of the Homunculus nebula; (3) scattered emission from the southeast lobe (its counterpart for the northwest lobe is not seen in this element); (4) and (5) equatorial ejecta; and (6) and (7) the caps of the internal bipolar nebula.

We selected three strong, unblended [Fe II] lines at $\lambda\lambda$4891, 4907, and 4975 Å (vacuum) for the following analysis in order to avoid possible spatial variations in different atomic species. At each slit position, the spectral images of these lines were then combined via a median-filter superposition to enhance faint velocity structures, as shown in the right panel of Figure 2. Furthermore, to emphasize the changes in *intrinsic emission* features, each composite spectral image was processed to suppress the broad stellar continuum scattered by dust in the Homunculus Nebula. Then apparent Doppler velocities were measured from line profiles extracted at numerous positions along the STIS slit (with a sampling width of five CCD rows, or 0.″25). Some spatial sampling may overlap slightly. Figure 4 shows an example of our velocity measurements taken at an offset 0.″4 in the southwest direction. Velocity widths may give some indication of the geometrical thickness of a nebular wall. In this image, a typical velocity width in the curve component is $\approx$91 km s^{-1}, although the value varies by 20 km s^{-1} both along the slit and at each pointing. The intrinsic velocity width is roughly 85 km s^{-1} after correction for instrumental resolution. These scans were done for the composite frames taken at 1.″5 away from the star in both the southwest and northeast directions. Beyond that distance, the emission structure became too faint to be detected with confidence.

We then combined the spectral mapping images to synthesize a velocity data cube. Since spatial coverage was not complete for the red (6490–7050 Å) data, a simple bilinear interpolation scheme filled the gaps (for more details see Ishibashi, Gull, & Davidson 2001). Each data cube allows us to visualize an extremely "narrowband" image, tunable in velocity to its pixel resolution, $\Delta V \approx$ 10–20 km s^{-1}. Our spectral resolution with the $52'' \times 0.''1$ slit was roughly 32 and 47 km s^{-1} for the blue and red data, respectively, with corresponding spatial samplings roughly $0.''05 \times 0.''1$ (blue) and $0.''25 \times 0.''1$ (red). Velocity cubes are plotted in Figures 5 and 6. The [Fe II] λ4891 maps shown in Figure 5 demonstrate that a narrowband image with subarcsecond spatial resolution can be synthesized from data obtained with a narrow-slit spectrograph on the *HST*. Each data set allows us to investigate spatial structures of emission in a single atomic line. Each of the [Fe II] lines mentioned above individually gives practically identical results. The removal of scattered light originating from the extended nebula also simplifies the examination of faint nebular condensations.

Figure 6 shows 40 panels of narrowband maps covering the range from -955 to $+1022$ km s^{-1} for the Hα emission line, just to demonstrate the amount of kinetic information that can be gathered by the mapping observation. In this velocity range, the neighboring [N II] emission lines contribute significantly to the intensity near -670 and $+940$ km s^{-1}. These narrowband maps may be useful for future studies of the scattered emission structure of the Homunculus and intrinsic emission from shells and strings in the outer halo. To our knowledge, no previous instrument has ever achieved these levels of angular and spectral resolution simultaneously (see Davidson et al. 1997 for a comparable instance using an earlier *HST* instrument).

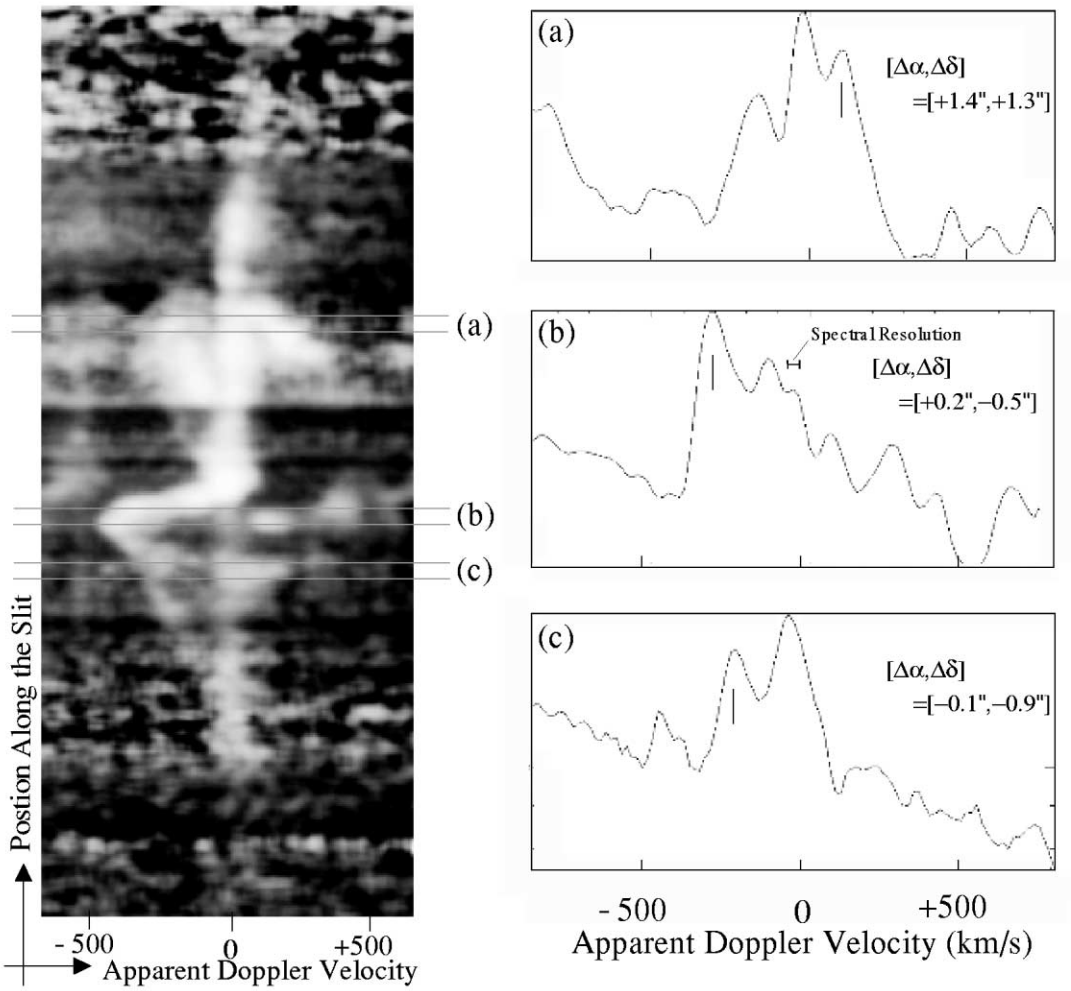

FIG. 4.—Tracings of the narrow emission lines at three locations along the slit positioned at an offset 0″.4 in the southwest direction. Spatial coordinate for each spectral sample is given as an offset from the star in arcseconds. Positive $\Delta\alpha$ values refer an offset toward the east (along the right ascension), while positive $\Delta\delta$ values refer to an offset toward the north (along the declination). Short vertical lines indicate narrow emission lines associated with the curve component.

4. RECONSTRUCTION OF THE INTERNAL NEBULAR STRUCTURE

Our goal here is to derive the geometrical structure of the inner bipolar emission nebula: the curve component in Figure 2, or features 6 and 7 in Figure 3. Results can then be compared to the larger bipolar shapes and equatorial structures assessed by Davidson et al. (2001). As usual for studies of the Homunculus, we assume (1) that all these ejecta originated from the central star, and (2) that they are moving ballistically without significant deceleration. We measured apparent heliocentric Doppler velocities and then, consistent with Davidson et al., we added +10 km s^{-1} as a crude but adequate correction for the systemic velocity of η Car. From the resulting velocity V_z parallel to our line of sight we calculate the "distance from the plane of the sky" $z = V_z t$, i.e., a relative linear coordinate along the line of sight, where t is the age of the ejecta.

4.1. *Proper Motion and Age Determination*

Figure 3 contains a hint that the standard ejection date of large Homunculus lobes, around the year 1843 (Morse et al. 2001; Currie & Dowling 1999), is not appropriate for the Little Homunculus. Slopes of loci in this figure depend on the expansion age. As explained by Davidson et al. (2001), approximate axial symmetry makes the outer polar caps (segments 1 and 2 in Fig. 3) parallel to the main equatorial debris (segment 4). The inner structures 6 and 7, however, have a very different slope in Figure 3, more or less parallel to segment 5, which probably represents younger equatorial ejecta from the 1890 outburst or later. Thus, we have reason to suspect that the inner mini-Homunculus was ejected later than the well-known outer lobes.

Proper motions give a more specific estimate of t. For this purpose we compared the 1998 March 19 and 2000 March 20 data sets (Table 1). Careful cross-correlations along the slit direction showed a small but measurable spatial drift of the northwest part of the curve component in Figure 2. In order to minimize contamination by the large-scale Homunculus and the bar component, we used small 0″.51 and 0″.63 square sample sizes for the correlation. The procedure addressed, separately, 28 [Fe II] lines and the bright [Ni II] λ7379.86 (vacuum) feature. The southeast segment of the curve component could not be used, as the selected lines were generally too weak there. For each emission line, the expansion age was determined. This analysis showed ejection years 1904 $\pm$ 10 and 1897 $\pm$ 10 using the 0″.51 and 0″.63 sampling boxes, respectively (see Fig. 7). Here the quoted 1 σ errors are dominated by a general $\pm$10 km s^{-1} velocity uncertainty and also include the formal dispersion of the

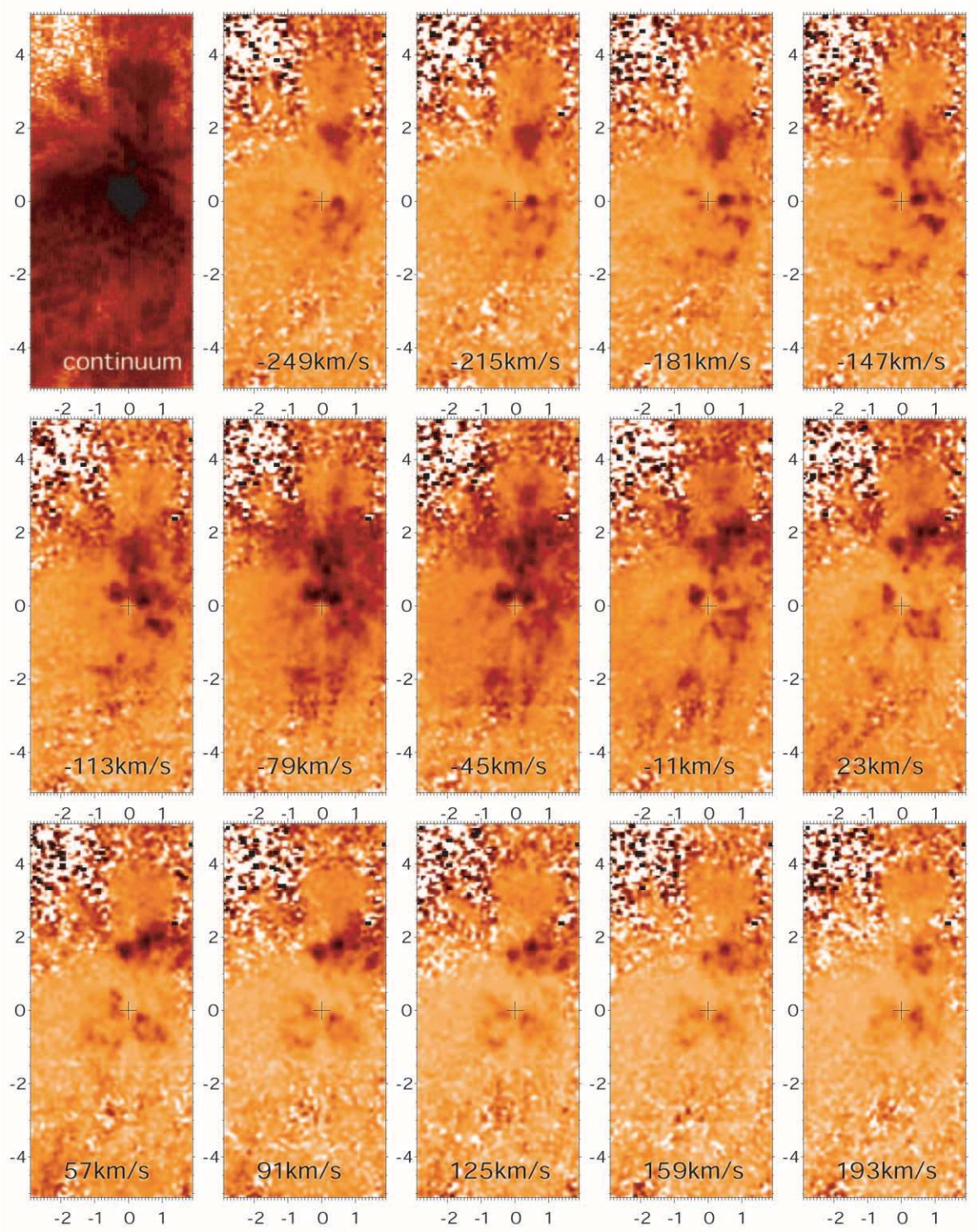

FIG. 5.—Velocity maps of [Fe II] λ4891 (vacuum) emission in intervals of 34 km s^{-1} between -249 and $+193$ km s^{-1}. A brighter nebular condensation appears darker in the image. Any true emission feature would appear as a smooth feature in these panels, whereas a noticeable "salt and pepper" noise appears in the upper left corner of each image. For a visual aid, a broadband continuum image of η Car, synthesized from the mapping velocity cube, is shown in the upper left panel. A crosshair (0.″5 in diameter) in each panel indicates the position of the bright central source. Note that the central star is surrounded by a torus-like ring emission 0.″5 in diameter. The scale of both axes is in units of arcseconds, with the central star at its origin.

individual line measurements. It is not surprising that the larger sampling size gave a larger age, since it presumably has more contamination by ejecta from the major circa 1843 event. These results are quite independent of the deduction expressed in the preceding paragraph, and are consistent with it. Therefore (rounding somewhat for simplicity), we adopt $t \approx 100$ yr for the inner structure.

4.2. *The Little Homunculus*

Figure 8 shows the bipolar emission nebula projected on the plane of the major axis of the Homunculus, based on the 2000 March 13 data. One unit (arcsec) on either axis corresponds to a linear distance of 2250 AU $= 3.37 \times 10^{16}$ cm if the distance of η Car is 2250 pc. The outer Homunculus lobe

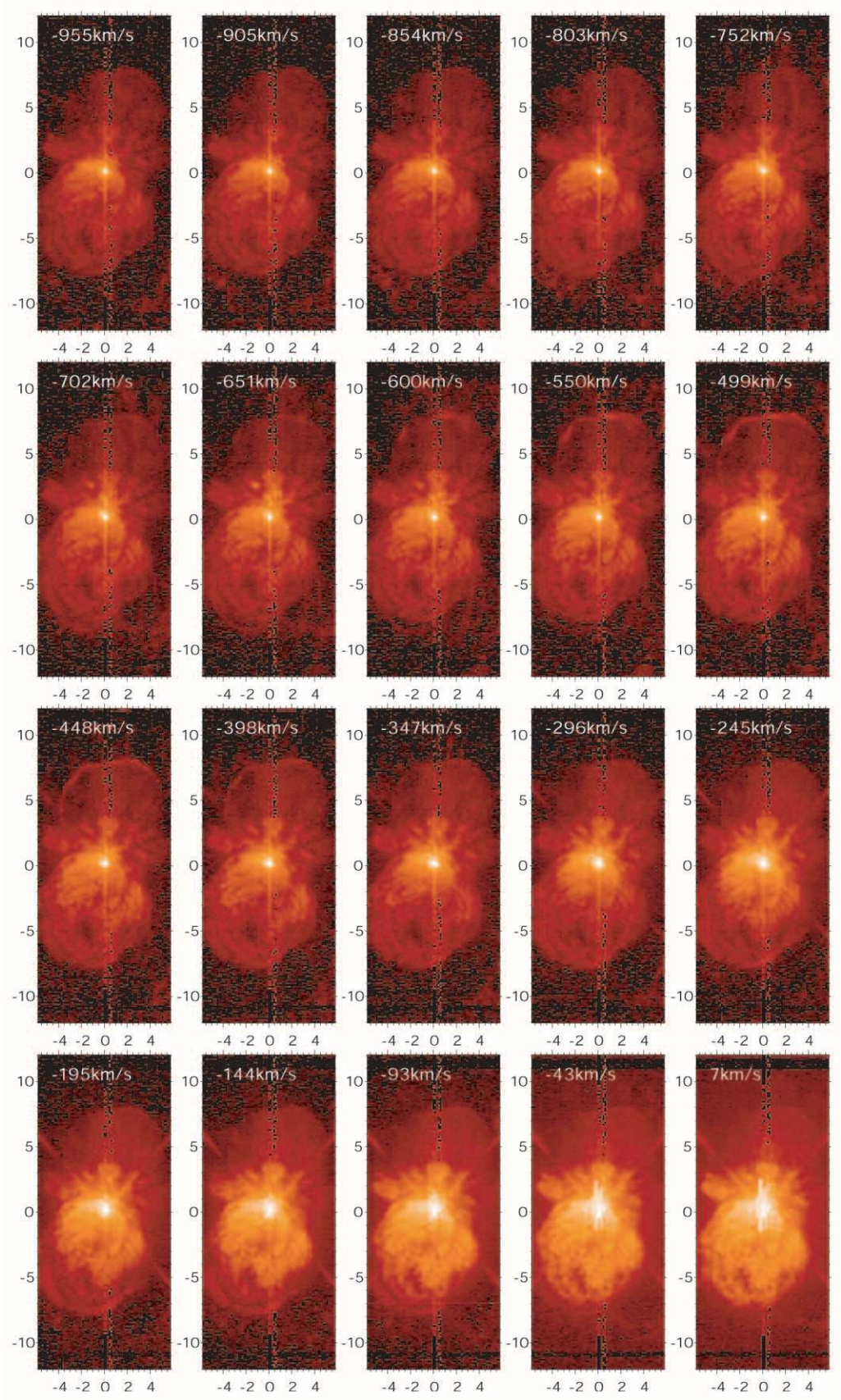

FIG. 6.—Velocity maps of Hα emission in intervals of 50.7 km s^{-1} between -955 and $+1022$ km s^{-1}. A brighter nebular emission (both scattered and intrinsic) appears brighter in the scale. A vertical stripe across the central source is an artifact due to the image synthesis. Some panels show saturation near the star as well. The cross pattern that intersects at the position of the star is a diffraction pattern of the *HST* optics. The scale of both axes is in units of arcseconds, with the central star at its origin. All panels include part of the [N II] emission features adjacent to Hα.

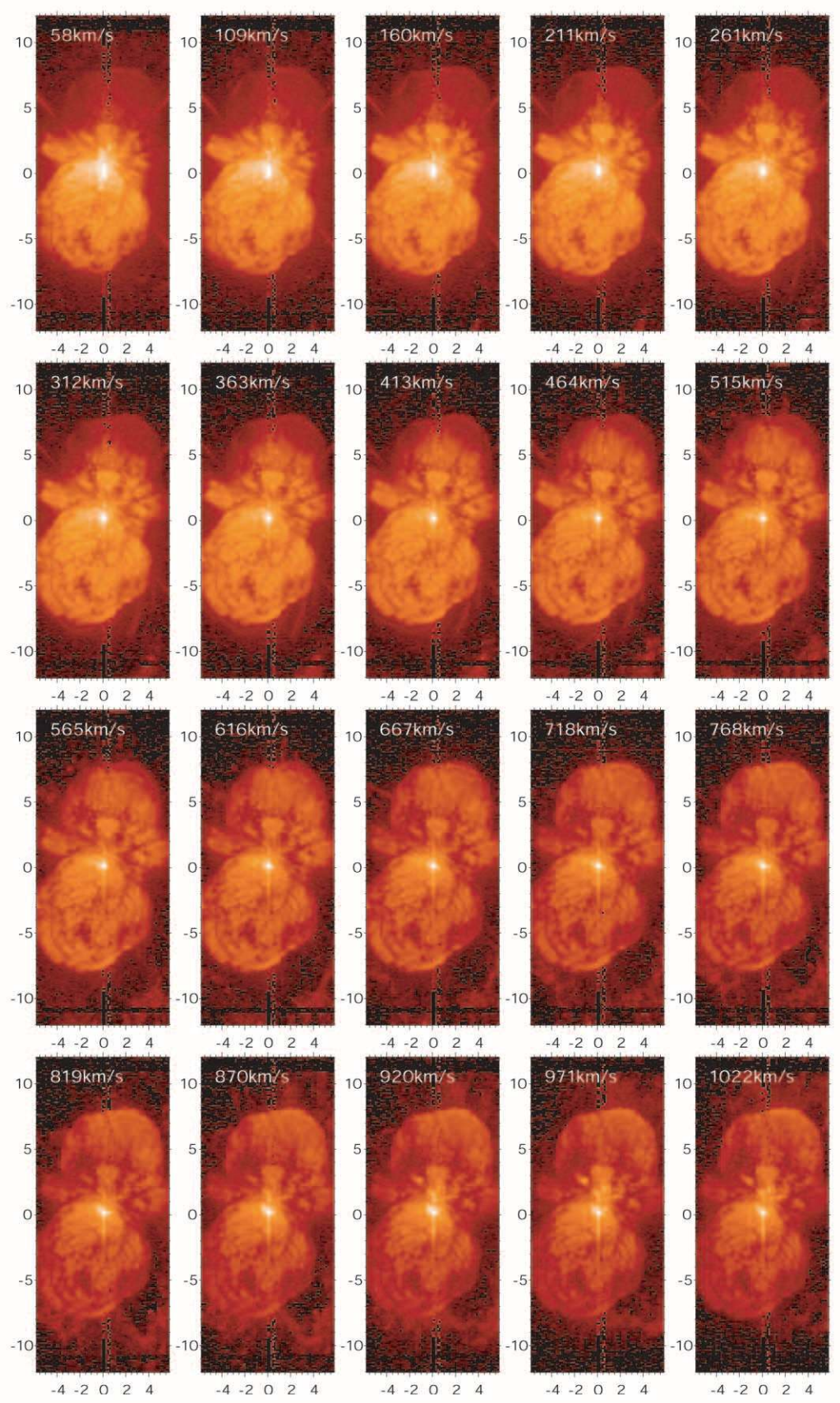

FIG. 6.—*Continued*

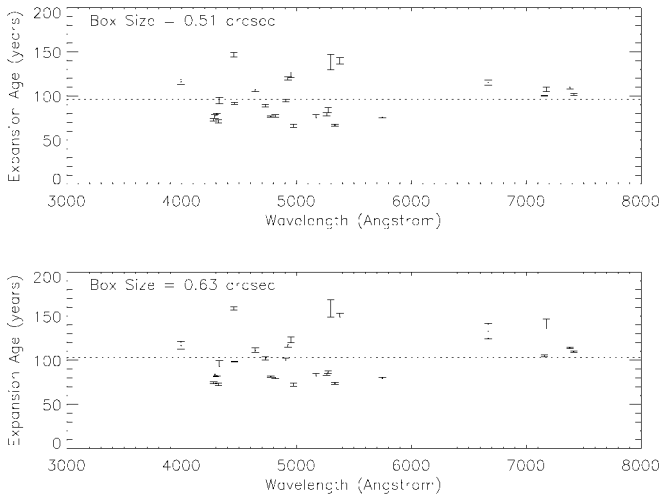

FIG. 7.—Measured expansion age of the Little Homunculus. Error bars represent $\pm\sigma$ uncertainty in measurement. The dotted line indicate the mean of expansion age.

shapes marked by plus signs in Figure 8 (from Davidson et al. 2001) are based on an age of 157 yr; however, for the inner structure marked with dots, we assume $t = 100$ yr, as explained above. Like the familiar Homunculus, the embedded bipolar nebula appears to be "approximately" hollow, i.e., some lower density material exists inside it but the shell surface is well defined (Davidson et al. 2001; Smith, Gehrz, & Krautter 1998; Smith et al. 1995). Its polar caps are expanding outward at about 300 km s^{-1}, about half as fast as the large Homunculus lobes. We refer to this quasi-hollow inner structure as the Little Homunculus.[19]

[19] Another proposed name was "Matryoshka" (nesting doll, literally "little mother," Russian).

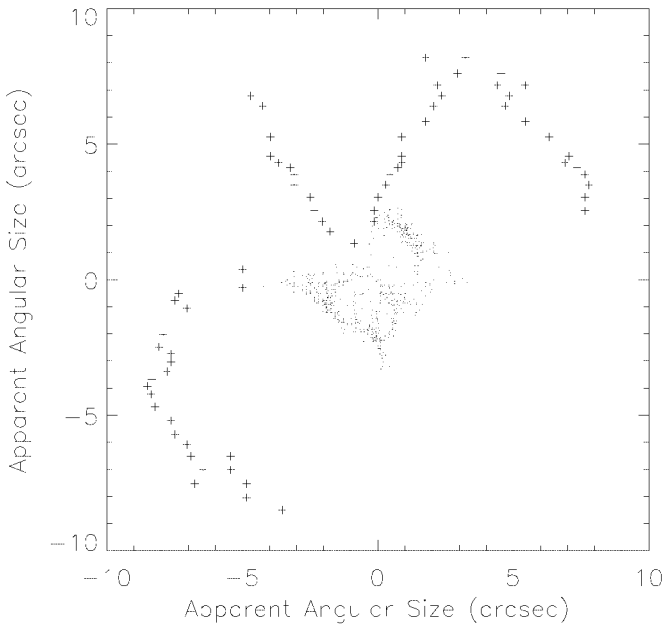

FIG. 8.—Two-dimensional slice image of the Homunculus and the Little Homunculus. Small dots and plus signs are data points taken from the images of the Little Homunculus and the Homunculus, respectively.

Figure 9 illustrates a preliminary result of three-dimensional reconstruction of [Fe II] λ4891 (vacuum) emission structure in the Little Homunculus nebula, based on the mapping data set. A bipolar-like nozzle segment of the internal nebula is clearly present in this viewing angle, although the presented three-dimensional data cube suffers from the low signal-to-noise ratio in these data.

4.3. *The Bar Component*

The physical nature of the bar component in Figure 2 is not clearly understood. We speculate that it is spatially detached from both the large Homunculus and the little one. A similar radiative pumping mechanism probably excites the spectra of the Weigelt blobs, the curve component, and the bar component, since all three structures share the same, somewhat unusual set of strongest emission lines. Furthermore, from its constant, extremely narrow velocity structure across the slit position, our first impression of its geometry is a thin shell embedded within an outer diffuse gas in the equatorial region of the system (equatorial halo may be a valid description). If the bar component were physically located within the Homunculus or coincided with the Little Homunculus, then changes in velocity would have been expected across the position of the central star. However, such changes were not detected (Ishibashi 1999). Thus, it seems more appropriate to consider the presence of outer or extended diffuse gas that is radiatively excited by scattered UV photons in the equatorial region. We attempt to illustrate both the curve and bar components in a cartoon model of the η Car nebula (see Fig. 10).

5. PHYSICAL CONDITIONS IN THE LITTLE HOMUNCULUS

Figure 11 shows a spectrum of the Little Homunculus sampled 1.″53 from the central star at P.A. 332.°1, with a 0.″1 × 0.″13 rectangular aperture. It exhibits a forest of narrow emission lines like other nebular condensations around the star. In general, the excitation mechanisms of these lines are not well understood; high levels of Fe II are populated by radiative pumping, while the lower levels may be collisionally excited at temperatures of a few thousand K (Johansson & Zethson 1999). Fortunately, however, the gas densities are sufficiently high that many lower, metastable level populations may be close to a quasi-Boltzmann distribution. Therefore, we employ a simple technique first applied to η Car by Pagel (1969) and more recently used by Davidson et al. (1995) and Hamann et al. (1999). We consider only forbidden [Fe II] lines that have fairly low critical densities ($\sim 10^6$ cm^{-3}; see Hamann et al. 1999), and we suppose that their upper levels are populated according to an idealized Boltzmann distribution at some fixed temperature; then the observed *relative* line intensities depend on temperature and on reddening by dust. The validity of these assumptions can be judged by the mutual consistency of many different line intensities.

Step 1.—We selected 38 unblended [Fe II] lines in the wavelength range 4100–9000 Å and measured their apparent intensities. These measurements and the atomic parameters are tabulated in Table 2. Decay rates for [Fe II] lines are quoted from the relativistic Hartree-Fock calculation by Quinet, Le Dourneuf, & Zeippen (1996). We exclude 4 of the 38 measured lines from the following analysis because

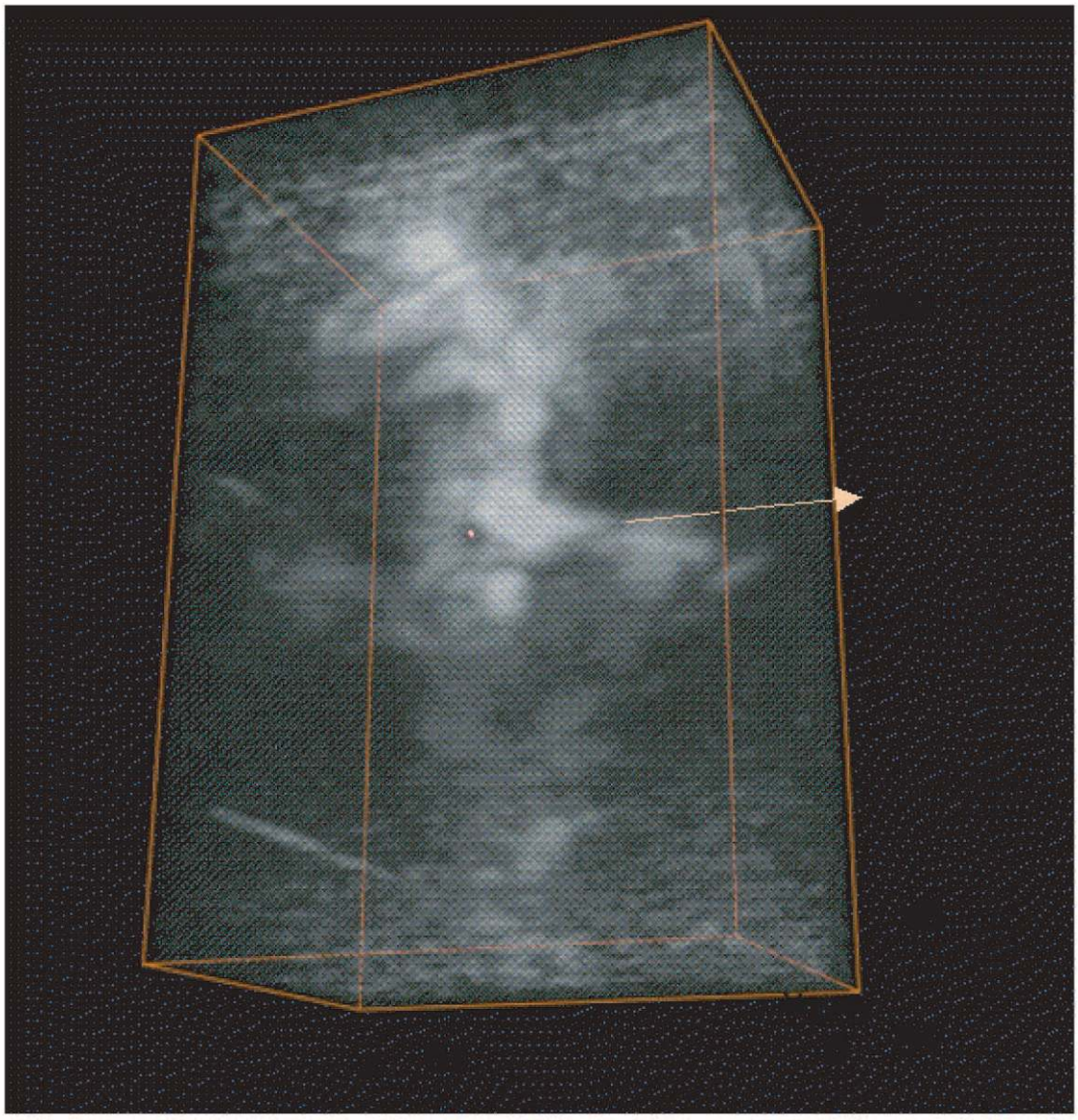

FIG. 9.—Three-dimensional structure of [Fe II] λ4891 (vacuum). The position of the star is indicated by a dot inserted in the image. The angular dimension of the box is roughly $7'' \times 10'' \times 5''$ (width $\times$ height $\times$ depth). The arrow indicates the direction toward the observer. Bright features are shown in white. A bipolar nozzle-like structure corresponds to the Little Homunculus. Because of the poor signal-to-noise ratio in the data set, only a part (primarily the near-side only) of the inner lobe structure is seen. Volume rendering is performed with the AnimaBob graphic package.

their decay rates are doubtful (marked as 1 in Flag column in Table 2; see "Note added to the proof" in Quinet et al.). Hence, we use 34 [Fe II] measurements in the following steps.

Step 2.—We have

$$I_{\rm obs} = C_1 \epsilon_{ij} A_{ji} g_j e^{-\epsilon_j/kT} e^{-\tau} ,$$

where $I_{\rm obs}$ is an observed line intensity, C_1 is a constant, ϵ_{ij} and A_{ji} are the photon energy and decay rate for the transition from levels j to i, ϵ_j and g_j are the energy and statistical weight of the upper level j, and τ is a wavelength-dependent effective optical depth due to absorption and scattering by dust grains. Since extinction and reddening near η Car are too abnormal to represent with a standard curve (see below), we simply assume that τ is linear in $1/\lambda$ or in photon energy ϵ; this approximation is adequate for our purposes with most likely reddening curves. In order to give the correct reddening parameter E_{B-V} expressed in astronomical magnitudes, the linear relation must be

$$\tau(\epsilon) \approx C_2 + \left(\frac{\epsilon}{0.58 \text{ eV}} \right) E_{B-V} .$$

Thus, we can rewrite the earlier equation in a practical form:

$$\ln\left(\frac{\epsilon_{ij} A_{ji} g_j}{I_{\rm obs}} \right) \approx C_3 + \left(\frac{1}{kT} + \frac{\epsilon_{ji}}{\epsilon_j} \frac{E_{B-V}}{0.58 \text{ eV}} \right) \epsilon_j ,$$

which can be further simplified as

$$\approx C_3 + \left(\frac{1}{kT} + \frac{E_{B-V}}{0.66 \text{ eV}} \right) \epsilon_j ,$$

since the ratio ϵ_{ji}/ϵ_j in Table 2 is always 1 or slightly less than

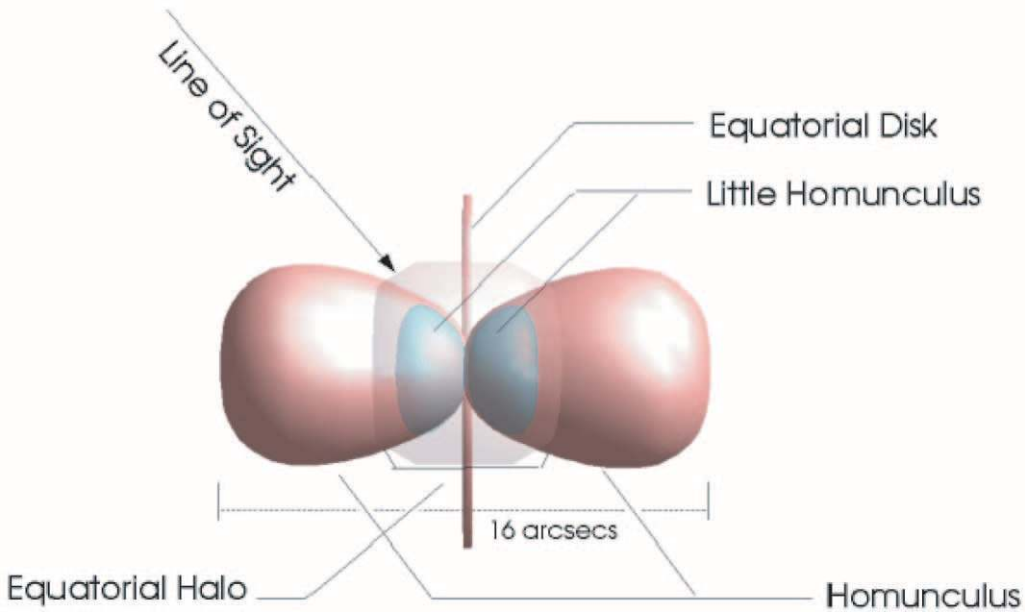

FIG. 10.—Cartoon model of the η Car Nebula

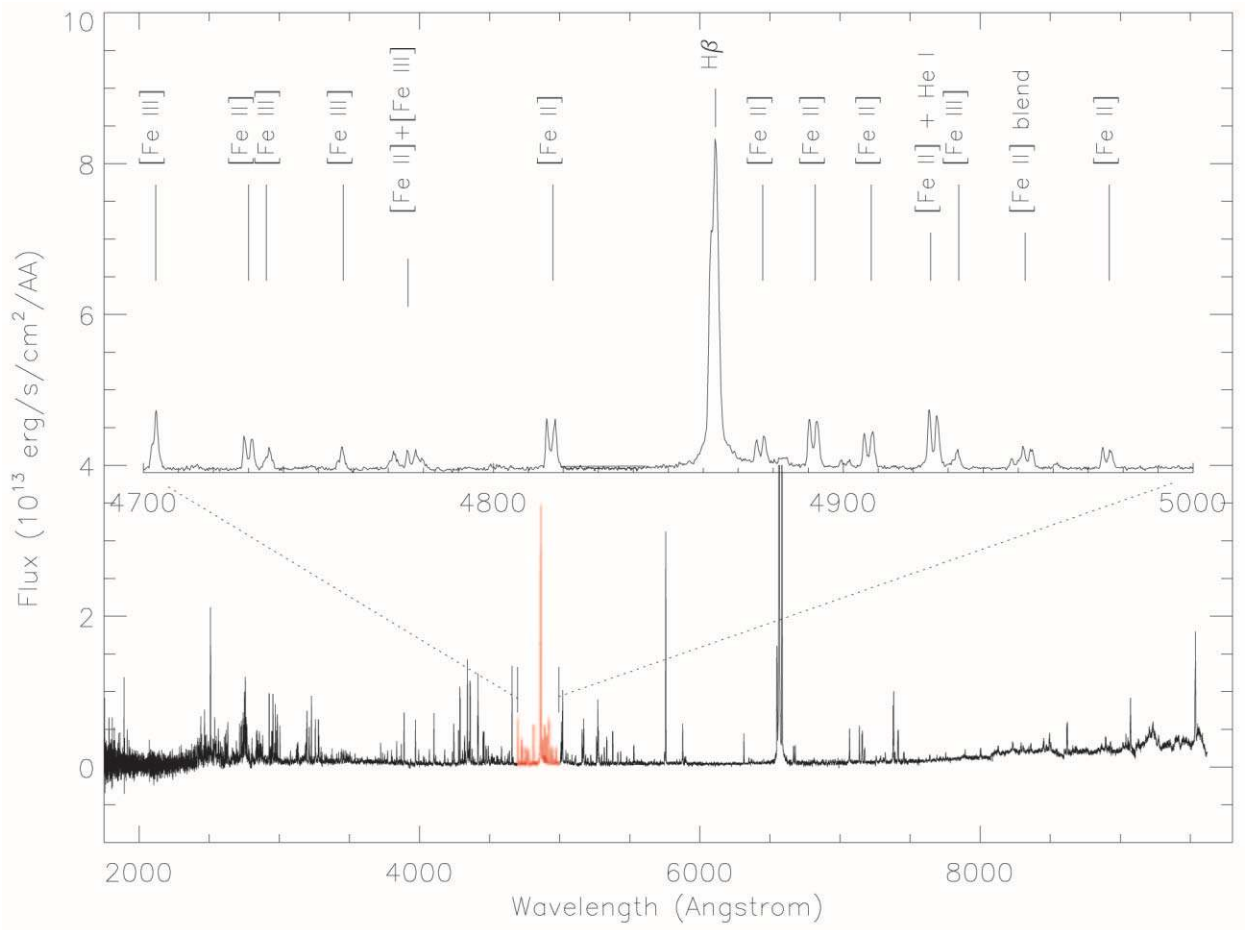

FIG. 11.—NUV/Visual spectrum of the Little Homunculus taken in the 2000 March 20 visit. A part of the spectrum (drawn in red) is magnified to show the detail of observed line profiles.

TABLE 2
OBSERVED [Fe II] LINE INTENSITIES FROM THE LITTLE HOMUNCULUS

λ_{obs}[a] (Å)	λ_{rest}[a] (Å)	ϵ_j (eV)	I_{obs} (10^{-14} ergs s^{-1} cm^{-2})	A_{ji}	g_j	Multiplet	Notes[b]
4116.99	4115.63	3.245	1.10	0.103	12	$23F\,a^4F–b^2H$	
4279.44	4278.03	3.199	5.82	0.819	10	$21F\,a^4F–a^4G$	
4289.99	4288.60	2.891	13.0	1.650	6	$7F\,a^6D–a^6S$	
4308.29	4307.10	3.230	2.01	0.388	6	$21F\,a^4F–a^4G$	
4322.22	4320.84	3.221	3.83	0.658	8	$21F\,a^4F–a^4G$	
4349.49	4348.07	3.153	1.88	0.250	12	$21F\,a^4F–a^4G$	
4355.40	4354.00	3.199	3.90	0.380	10	$21F\,a^4F–a^4G$	
4375.09	4373.66	3.221	2.58	0.340	8	$21F\,a^4F–a^4G$	
4385.55	4383.98	2.828	1.31	0.054	8	$6F\,a^6D–b^4F$	
4454.82	4453.35	2.891	5.49	0.548	6	$7F\,a^6D–a^6S$	
4460.71	4459.20	2.828	5.89	0.279	8	$6F\,a^6D–b^4F$	
4642.51	4640.97	2.778	2.02	0.499	2	$4F\,a^6D–b^4P$	
4731.01	4729.39	2.704	4.50	0.478	4	$4F\,a^6D–b^4P$	
4817.51	4815.88	2.807	7.44	0.521	10	$20F\,a^4F–b^4F$	
4877.41	4875.85	2.844	3.33	0.223	6	$20F\,a^4F–b^4F$	
4892.48	4890.98	2.583	7.04	0.347	6	$4F\,a^6D–b^4P$	2
4908.31	4906.70	2.838	5.56	0.285	8	$20F\,a^4F–b^4F$	
4976.34	4974.78	2.844	3.21	0.183	6	$20F\,a^4F–b^4F$	
5046.51	5044.93	2.844	1.29	0.094	6	$20F\,a^4F–b^4F$	
5075.41	5073.80	2.676	0.48	0.028	10	$19F\,a^4F–a^4H$	
5161.69	5160.21	2.635	7.04	0.605	14	$19F\,a^4F–a^4H$	2?
5167.25	5165.39	3.387	3.77	0.309	8	$35F\,a^4D–a^2F$	
5185.30	5183.39	2.778	1.50	0.500	2	$18F\,a^4F–b^4P$	1
5223.35	5221.51	2.676	1.55	0.144	10	$19F\,a^4F–a^4H$	
5264.80	5263.09	2.657	5.77	0.429	12	$19F\,a^4F–a^4H$	
5300.23	5298.30	2.692	1.36	0.118	8	$19F\,a^4F–a^4H$	
5336.86	5335.13	2.676	4.83	0.351	10	$19F\,a^4F–a^4H$	
5379.69	5377.95	2.692	7.07	0.348	8	$19F\,a^4F–a^4H$	
5436.25	5434.64	2.583	2.32	0.174	6	$18F\,a^4F–b^4P$	1
5480.55	5478.76	3.339	1.29	0.448	2	$34F\,a^4D–b^2P$	
5750.39	5748.56	3.197	3.67	0.373	4	$34F\,a^4D–b^2P$	2
7159.37	7157.13	1.964	9.87	0.153	10	$14F\,a^4F–a^2G$	
7176.35	7173.98	2.030	3.75	0.059	8	$14F\,a^4F–a^2G$	
7392.69	7390.21	2.030	2.79	0.045	8	$14F\,a^4F–a^2G$	
7457.11	7454.59	1.964	3.21	0.049	10	$14F\,a^4F–a^2G$	
7642.04	7639.64	1.671	1.96	0.007	6	$1F\,a^6D–a^4P$	
8622.04	8619.32	1.671	12.6	0.031	6	$13F\,a^4F–a^4P$	1
8897.25	8894.35	1.695	9.20	0.020	4	$13F\,a^4F–a^4P$	1

[a] Wavelengths in vacuo.
[b] Notes: (1) lower quality A values; (2) possibly blended.

1. The median value of ϵ_{ji}/ϵ_j is about 0.88, and we apply this median value as a correction factor.

Figure 12 shows ϵ_j versus $\ln(\epsilon_{ij}A_{ji}g_j/I_{obs})$ for our 34 [Fe II] lines; the slope indicates that

$$\left(\frac{1}{kT}+\frac{E_{B-V}}{0.66\ \mathrm{eV}}\right)\approx 2.03\pm 0.22\ \mathrm{eV}^{-1}\ .$$

Evidently this gives a relation between consistent values of gas temperature T and reddening E_{B-V}.

Figure 13 shows the relation between E_{B-V} and T based on this analysis. The extinction-to-reddening ratio A_V/E_{B-V} is not known, but available studies find values around 4 or 5 for interstellar extinction of stars near η Car, and much greater for dust within the Homunculus itself (see many references cited in Davidson & Humphreys 1997). Interstellar reddening to the Carina Nebula is about 0.45 mag, and the corresponding extinction is roughly 1.7 mag (Walborn 1995). Earlier studies suggest that the reddening of the Weigelt blobs close to the star may be as small as 0.55 mag (Davidson et al. 1995). Therefore, it seems likely that the reddening for the Little Homunculus is in the neighborhood of $E_{B-V}\approx 0.5$ mag. Two vertical lines in Figure 13 indicate values of 0.45 and 0.55. This result suggests that the gas temperature of the Little Homunculus Nebula is likely to be found near 9000 K.

An order-of-magnitude particle density estimate is possible. At $T\sim 9000$ K, we assume an ionization fraction of Fe of approximately 30% and a reddening of $E_{B-V}=0.50$. The partition function varies with particle density (Traving, Baschek, & Holweger 1966): 68,000, 12,000, and 2200 for densities of 10^5, 10^6, and 10^7 cm^{-3}, respectively. In each case the observed brightness of the emission lines requires roughly 2×10^{50}, 3×10^{49}, and 6×10^{48} Fe atoms in the volume of $0\farcs1\times 0\farcs13\times 0\farcs5$ ($\sim 3\times 10^{47}$ cm^3), respectively. Comparing the derived densities with the assumed ones, the acceptable range of density n_H is roughly $10^6 < n_H < 10^7$ cm^3 if the Fe/H abundance is similar to the solar abundance. Suppose that the Little Homunculus consists of a bipolar cap within a radius $R=1\farcs5$ and thickness $\delta=0\farcs5$

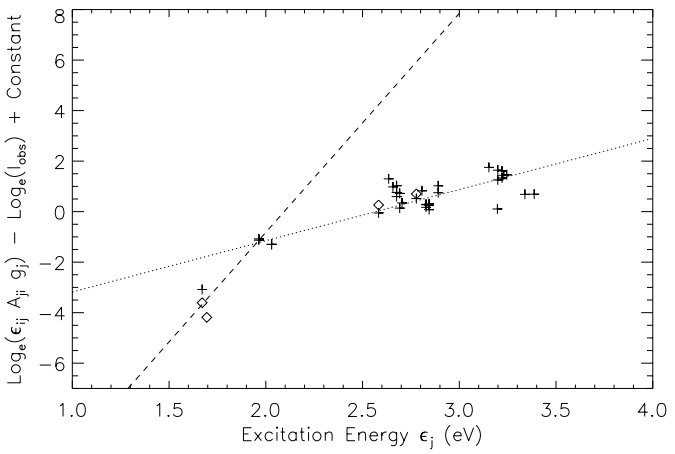

FIG. 12.—Excitation energy ϵ_j vs. $\ln(\epsilon_{ij}A_{ji}g_j) - \ln(I_{obs})$. The dotted line indicates the best linear fit through good data points (*plus signs*). Four data points, not included in the best fit, are marked with diamonds. If these four data points are included, then the slope of the fit through the lowest levels (*dashed line*) is much higher, 8.67 ± 1.73 eV^{-1}. This value is so large that it requires very high values of E_{B-V}, which are not plausible.

(imagine a "disklike" cap). Further assume its filling factor to be unity. Then the total mass is estimated as 0.1 $M_\odot$ for $n_H = 10^6$ cm^{-3} and 1 $M_\odot$ for $n_H = 10^7$ cm^{-3}. At the distance of $\sim 2''$ ($\sim$4500 AU) from the star, the radiation-density temperature of the nebula is roughly 280 K, assuming that the effective temperature of η Car's atmosphere at 60 $R_\odot$ is $\sim$35,000 K (Hillier et al. 2001). This temperature is slightly warmer than that of the Homunculus ($\sim$200 K). If the Little Homunculus contains a mass of 1 $M_\odot$ of gas, it may contain roughly 0.01 $M_\odot$ of dust. Such a mass of dust in the nebula would give rise to a bright thermal IR source with a color temperature of 280 K, and therefore the nebula should be detected clearly in earlier IR images. However, this is not known to be the case (Smith et al. 2002). So intuitively, the total mass of the Little Homunculus (at least the cap part) should be much less than 1 $M_\odot$, implying that either the density n_H is lower than 10^7 cm^{-3} or its filling factor is much less than unity. Other factors (a supersolar Fe/H ratio, etc.) may effectively lower the total mass of the Little Homunculus as well.

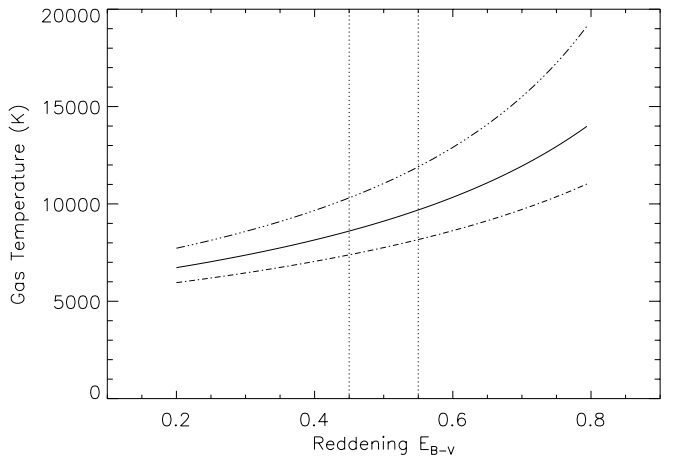

FIG. 13.—Reddening E_{B-V} vs. gas temperature T. The solid curve is derived based on the slope of the best fit given in Fig. 12. The other two dot-dashed curves define the upper and lower boundary conditions given by the uncertainty of the fit. The vertical dotted lines mark the range of E_{B-V} that has been generally accepted in previous studies.

5.1. *Temporal Variability of the Little Homunculus*

Using three data sets obtained at the same position angle but at different epochs, we also examine temporal variability of the Little Homunculus. Spectral samples were taken for 18 emission lines of [Fe II], Fe II, and [Ni II] and integrated line fluxes were measured for each epoch at the star, Weigelt blobs B and D, and the cap of the Little Homunculus for comparison. None of the selected lines were high-excitation species (e.g., [Fe III]) that require a very intense, ionizing UV radiation field. High-excitation lines are also known to be susceptible to η Car's 5.5 yr periodic cycle. The flux ratios measured for these low-excitation lines are plotted in Figure 14.

Two physically independent variations were present during the period monitored with STIS: the changes due to the 5.5 yr periodic variability (Damineli 1996) and the recently discovered brightening of the stellar source at visual wavelengths (Davidson et al. 1999). The effect of the recent brightening is illustrated well in the top panel of Figure 14, showing that the stellar flux has increased by an appreciable factor. However, both Weigelt blobs and the Little Homunculus remained fairly constant in their line emission strengths during the event and afterward.

On the other hand, high-excitation line species in the nebula exhibit strong variability throughout our monitoring. High-excitation lines at the cap during the last event were all weaker, following a trend similar to that seen in the Weigelt blobs. Figure 15 illustrates the change in

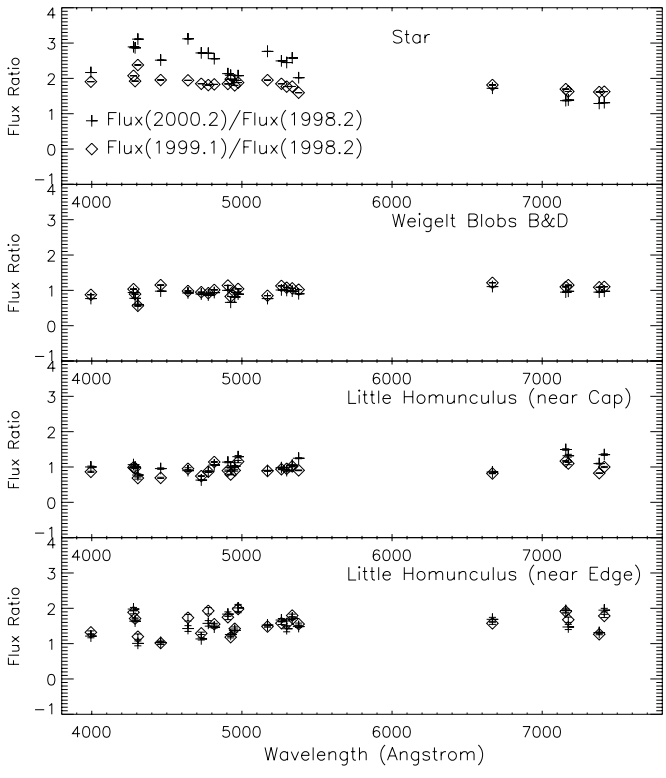

FIG. 14.—Temporal variations seen in the [Fe II] and [Ni II] line fluxes of stars, Weigelt blobs, and the Little Homunculus. Spectral samples of the Little Homunculus were taken from the brightest part (called the "cap") and near the junction of the Homunculus Nebula and the Little Homunculus Nebula ("edge").

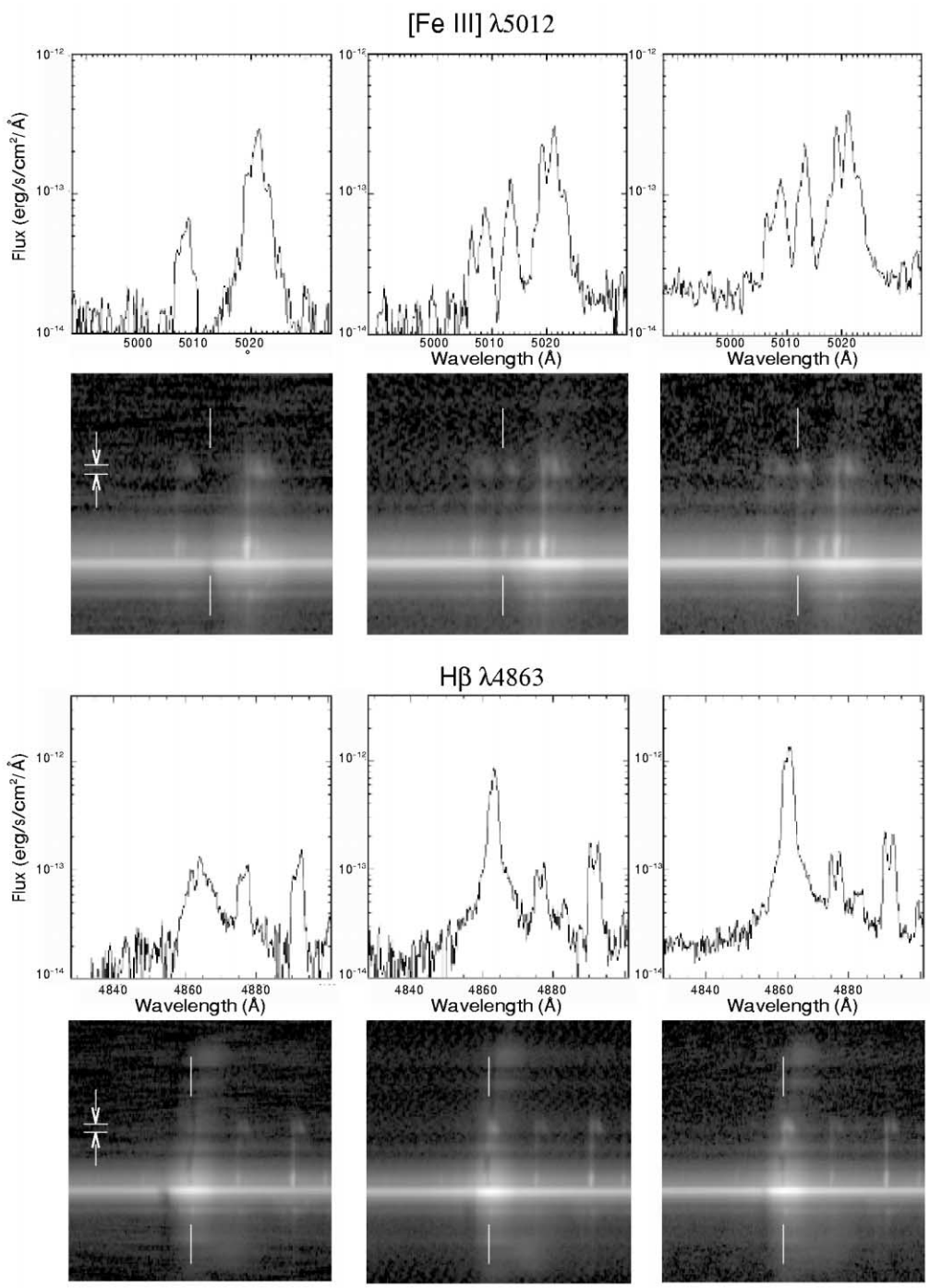

FIG. 15.—[Fe III] and Hβ spectra taken in 1998 March (*left*), 1999 February (*middle*), and 2000 March (*right*). The corresponding spectral images are also shown. Both [Fe III] and Hβ emission structures are marked with two vertical ticks on the spectral images. The spectral extraction width used to obtain the spectra are also marked. These high-excitation species require the presence of strong ionizing UV radiation in the field, and therefore are very sensitive to the periodic variation associated with the 5.5 yr event of η Car. Note that the bar component in [Fe II] appears to shift redward slightly as it extends outward, whereas the neighboring [Fe II] lines appear to show a near-constant velocity structure.

[Fe III] and Hβ lines.[20] The presence of Hβ in emission from the Little Homunculus indicates that hydrogen atoms are present in the ejecta. Presumably, UV photons may drive the enhanced strong high-excitation lines via UV pumping and two-photon excitation mechanism in the Weigelt blobs and other parts of the nebula, according to recent studies on atomic physics (Johansson & Hamann 1993). Assuming that this is the driving mechanism for high-excitation emission lines, our data suggest that changes in the UV ionizing radiation field may occur in both polar and equatorial directions. Naively, it may be an indication of the *isotropic* change in the ionizing UV radiation density field, although it certainly does not preclude any other possibilities (cf. Smith 2002).

[20] Note that the bar component in [Fe III] line is rather tilted; this appears to be true for all the high-excitation lines. This may indicate that [Fe III] lines in the bar component form at a closer distance to the star than [Fe II] or [Ni II] lines, possibly implying that the curvature of the [Fe III] line formation layer is much greater (i.e., the line formation occurs at a smaller radius centered at the star). This issue will be discussed in a future publication.

In turn, this implies that the 5.5 yr periodic event of η Car is driven by gross attenuation of the UV light in the same isotropic manner.

6. FINAL REMARKS

We have identified a Little Homunculus embedded within the Homunculus Nebula around η Car. The existence of this nebula perhaps could have been detected with the narrow-band *HST* WFPC2 imaging of η Car, as the blue glow shown in Figure 4 of Morse et al. (1998) suggested the presence of the peculiar hazy structure. However, two-dimensional imaging could not have resolved its complex three-dimensional structure, nor could it easily bring out a fainter emission structure over the bright scattered continuum emission from the Homunculus Nebula.

As explained in § 4 above, the age of the Little Homunculus appears to be about 100 yr. This is not a trivial finding. Smith & Gehrz (1998) first argued that the equatorial ejecta came from the 1890 eruption, but Morse et al. (2001) were unable to detect any ejecta coming from the 1890 eruption event based on the *HST* WFPC2 data sets. STIS spectra studied by Davidson et al. (2001) showed that the equatorial region may contain material from *both* the 1890 eruption and the Great Eruption in the 1840s. Our paper does not settle the debate on the age of the equatorial ejecta, but we deduce that some additional ejecta inside the Homunculus came from the minor eruption 50 yr after the Great Eruption.

The other controversy in η Car to date is whether it has a binary companion. This study does not settle the issue, as the large-scale nebula would see more or less a pointlike ionizing UV source at the heart of the stellar system regardless of whether there is a single star or a close binary system. However, from temporal variations seen in the Weigelt blobs (conceivably on the equatorial plane; see Davidson et al. 1995, 1997; Falcke et al. 1996) and the Little Homunculus, the changes in ionizing UV radiation flux may possibly occur in all directions (one of us [N. S.] has recently found strong evidence that changes in the UV flux are not isotropic; see Smith 2002). In the single-star case, this is what one would naturally expect. In the binary case, however, a simple hypothesis of "line-of-sight" eclipsing does not predict isotropic changes (cf. Ishibashi et al. 1999). However, a companion star may be submerged within the changing wind of η Car. This type of binary model has been discussed and is plausible (Davidson 1999; Damineli, Lopes, & Conti 1999 and references therein).

Whatever the true nature of η Car may be, we are still in the process of determining what we understand and what we do not. We are taking the next step by sorting out emission from several spatial structures and by examining the radiation mechanisms of the nebular condensations surrounding this very massive star.

K. I. held a National Research Council (NASA/GSFC) Research Associateship. N. S. was supported by a NASA/GSRP fellowship from NASA/GSFC. Additional funding was provided by NASA grants GO-7302 and GO-8327 (PI: K. Davidson) from the Space Telescope Science Institute, which is operated by the Association of Universities for Research in Astronomy, Inc., under NASA contract NAS5-26555, and by STIS IDT funding. We also thank D. H. Porter and P. R. Woodward at Laboratory for Computational Science and Engineering at University of Minnesota for providing support for three-dimensional visualization and volume rendering performed with AnimaBob graphic package.

REFERENCES

Currie, D. G., & Dowling, D. M. 1999, in ASP Conf. Ser. 179, Eta Carinae at the Millennium, ed. J. A. Morse, R. M. Humphreys, & A. Damineli (San Francisco: ASP), 72
Damineli, A. 1996, ApJ, 460, L49
Damineli, A., Lopes, D. F., & Conti, P. S. 1999, in ASP Conf. Ser. 179, Eta Carinae at the Millennium, ed. J. A. Morse, R. M. Humphreys, & A. Damineli (San Francisco: ASP), 288
Davidson, K. 1999, in ASP Conf. Ser. 179, Eta Carinae at the Millennium, ed. J. A. Morse, R. M. Humphreys, & A. Damineli (San Francisco: ASP), 304
Davidson, K., Ebbets, D., Weigelt, G., Humphreys, R. M., Hajian, A. R., Walborn, N. R., & Rosa, M. 1995, AJ, 109, 1784
Davidson, K., & Humphreys, R. M. 1997, ARA&A, 35, 1
Davidson, K., Smith, N., Gull, T. R., Ishibashi, K., & Hillier, J. D. 2001, AJ, 121, 1569
Davidson, K., et al. 1997, AJ, 113, 335
———. 1999, AJ, 118, 1777
Falcke, H., Davidson, K., Hofmann, K.-H., & Weigelt, G. 1996, A&A, 306, L17
Gaviola, E. 1950, ApJ, 111, 408
Gull, T. R., Ishibashi, K., & Davidson, K. 1999, in ASP Conf. Ser. 179, Eta Carinae at the Millennium, ed. J. A. Morse, R. M. Humphreys, & A. Damineli (San Francisco: ASP), 144
Gull, T. R., Taylor, M. J., Shaw, R., Robinson, R., & Hill, R. S. 1997, in 1997 *HST* Calibration Workshop with a New Generation of Instruments, ed. S. Casertano (Baltimore: STScI), 106
Hamann, F., Davidson, K., Ishibashi, K., & Gull, T. R. 1999, in ASP Conf. Ser. 179, Eta Carinae at the Millennium, ed. J. A. Morse, R. M. Humphreys, & A. Damineli (San Francisco: ASP), 116
Hillier, D. J., Davidson, K., Ishibashi, K., & Gull, T. 2001, ApJ, 553, 837
Humphreys, R. M., Davidson, K., & Smith, N. 1999, PASP, 111, 1124
Ishibashi, K. 1999, Ph.D. thesis, Univ. of Minnesota
Ishibashi, K., Corcoran, M. F., Davidson, K., Swank, J. H., Petre, R., Drake, S. A., Damineli, A., & White, S. 1999, ApJ, 524, 983
Ishibashi, K., Gull, T. R., & Davidson, K. 2001, in ASP Conf. Ser. 242, Eta Carinae and Other Mysterious Stars: the Hidden Opportunities of Emission Line Spectroscopy, ed. T. R. Gull, S. Johansson, & K. Davidson (San Francisco: ASP), 71
Johansson, S., & Hamann, F. 1993, Phys. Scr., T47, 157
Johansson, S., & Zethson, T. 1999, in ASP Conf. Ser. 179, Eta Carinae at the Millennium, ed. J. A. Morse, R. M. Humphreys, & A. Damineli (San Francisco: ASP), 171
Kimble, R. A., et al. 1998, ApJ, 492, L83
Lindler, D. 1999, CALSTIS Reference Guide (http://hires.gsfc.nasa.gov/stis/docs/calstis/calstis.html)
Morse, J. A., Davidson, K., Bally, J., Ebbets, D., Balick, B., & Frank, A. 1998, AJ, 116, 2443
Morse, J. A., Kellogg, J. R., Bally, J., Davidson, K., Balick, B., & Ebbets, D. 2001, ApJ, 548, L207
Pagel, B. E. J. 1969, Nature, 221, 325
Quinet, P., Le Dourneuf, M., & Zeippen, C. J. 1996, A&AS, 120, 361
Ringuelet, A. E. 1958, Z. Astrophys., 46S, 276
Smith, C. H., Aitken, D. K., Moore, T. J. T., Roche, P. F., Puetter, R. C., & Piña, R. K. 1995, MNRAS, 273, 354
Smith, N. 2002, Ph.D. thesis, Univ. of Minnesota
Smith, N., & Gehrz, R. D. 1998, AJ, 116, 823
Smith, N., Gehrz, R. D., Hinz, P. M., Hoffmann, W. F., Mamajek, E. E., Meyer, M. R., & Hora, J. L. 2002, ApJ, 567, L77
Smith, N., Gehrz, R. D., & Krautter, J. 1998, AJ, 116, 1332
Traving, G., Baschek, B., & Holweger, H. 1966, Abh. Hamburger Sternw., 8, 3
Walborn, N. R. 1995, Rev. Mexicana Astron. Astrofis. Ser. Conf. 2, The Eta Carinae Region: A Laboratory of Stellar Evolution (Mexico, DF: Inst. Astron., UNAM), 51
Walborn, N. R., Blanco, B. M., & Thackeray, A. D. 1978, ApJ, 219, 498
Woodgate, B. E., et al. 1998, PASP, 110, 1183
Zethson, T., Johansson, S., Davidson, K., Humphreys, R.M., Ishibashi, K., & Ebbets, D. 1999, A&A, 344, 211